Ex Vivo Modeling of Perioperative Air Leaks in Porcine Lungs

Charles Klassen, Chad E. Eckert, Jordan Wong, Jacques P. Guyette, Jason L. Harris, Suzanne Thompson, Leonard J. Wudel, and Harald C. Ott

Abstract*—*Objective: **A novel *ex vivo* model is described to advance the understanding of prolonged air leaks, one of the most common postoperative complications following thoracic resection procedures. *Methods:* As an alternative to *in vivo* testing, an *ex vivo* model simulating the various physiologic environments experienced by an isolated lung during the perioperative period was designed and built. Isolated porcine lungs were perfused and ventilated during open chest and closed chest simulations, mimicking intra and postoperative ventilation conditions. To assess and validate system capabilities, nine porcine lungs were tested by creating a standardized injury to create an approximately 250 cc/min air leak. Air leak rates, physiologic ventilation, and perfusion parameters were continuously monitored, while gas transfer analysis was performed on selected lungs. Segmental ventilation was monitored using electrical impedance tomography. *Results:* The evaluated lungs produced flow–volume and pressure–volume loops that approximated standard clinical representations under positive (mechanical) and negative (physiological) pressure ventilation modalities. Leak rate was averaged across the ventilation phases, and sharp increases in leak rate were observed between positive and negative pressure phases, suggesting that differences or changes in ventilation mechanics may strongly influence leak development. *Conclusion:* The successful design and validation of a novel *ex vivo* lung model was achieved. Model output paralleled clinical observations. Pressure modality may also play a significant role in air leak severity. *Significance:* This work provides a foundation for future studies aimed at increasing the understanding of air leaks to better inform means of mitigating the risk of air leaks under clinically relevant conditions.**

***Index Terms*—Air leak, bioreactor, *ex vivo* perfusion, isolated lung model, tissue engineering.**

Manuscript received October 7, 2017; accepted March 18, 2018. Date of publication March 26, 2018; date of current version November 20, 2018. This work was supported by Ethicon, Inc, a Johnson & Johnson Company. *(Corresponding author: Harald C. Ott.)*

C. Klassen is with the IVIVA Medical, Inc.

C. E. Eckert, J. Wong, J. L. Harris, and S. Thompson are with the Ethicon, Inc, a Johnson & Johnson Company.

J. P. Guyette is with the Center for Regenerative Medicine, Massachusetts General Hospital.

L. J. Wudel is with the Surgical Services–Cardiothoracic Surgery, Wake Forest Baptist Health.

H. C. Ott is with the Division of Thoracic Surgery, Department of Surgery, Massachusetts General Hospital, Boston, MA 02114 USA (e-mail: hott@mgh.harvard.edu).

Digital Object Identifier 10.1109/TBME.2018.2819625

I. Introduction

PROLONGED air leaks (PALs) are one of the most common complications after pulmonary resections [1]. Most PALs develop immediately after surgical resection or during the first postoperative day. Several studies have shown that air leaks (in particular PALs) are associated with a variety of postoperative complications, such as increased risk of empyema [2], atelectasis, pneumonia [3], and mortality [4]. The Society of Thoracic Surgeons (STS) defines a PAL as an air leak extending the otherwise necessary length of stay. For lobectomy, this can be the 4th, 5th or 6th postoperative day based on different classifications [2], [3], [5]. Air leaks are associated with increased patient discomfort due to prolonged chest tube drainage and hospitalization and amplified health care costs due to increased use of inpatient and outpatient resources [3].

Numerous risk factors have been proposed to be associated with air leaks following thoracic surgery. These factors are diverse and include patient gender, presence of adhesions, presence of a pneumothorax or an incomplete fissure, upper lobectomy, performance of an anatomical resection, presence of chronic obstructive pulmonary disease, preoperative use of steroids, fragile or aged lung parenchyma, adhesions requiring mobilization of the lung, body mass index, surgical technique, the experience of the surgeon, chest tube management postoperatively (suction vs water seal), and rupture of pre-existing blebs [6]–[9]. Unfortunately, such factors are not fully predictive; additionally, since the standard of care often involves waiting for leaks to resolve, surgeons rarely re-operate to address PALs, thus further limiting knowledge around leak etiology. A deeper understanding of PAL etiology could help drive innovation in the treatment and care of PAL and may ultimately reduce and prevent their occurrence.

To date, surgical and benchtop models have suffered from limitations that hinder progress towards understanding and addressing PALs. Air leaks have been simulated in *in vivo* and *ex vivo* models, but studies showing the sources of air leaks, quantifying the volume and/or frequency of leaks, or investigating leaks under physiologically relevant mechanics and disease states are lacking [10]. *In vivo* models are often restricted to the use of young, healthy animals that are free of disease and are not generally at a high risk for leaks. Though these models closely reflect proper lung mechanics, they do not allow for direct observation of leak sites or quantification of leak rates. Existing *ex vivo* models permit direct visualization of the leak site and can

more easily quantify leak rates, but are often performed under ventilator-assisted breathing which does not have the same ventilation mechanics as physiological breathing. Neither method has been rigorously used to investigate possible stressors leading to air leaks such as cough or physiologic deep breathing.

Given the lower cost, ability to use non-dedicated animal tissue, and ability to directly visualize and quantify leaks, *ex vivo* isolated lung models offer the possibility of functional and biological testing in a controlled systematic manner. Such isolated lung models have been in use since at least 1989 [11]–[14], and more recent iterations [15]–[19] have advanced the quantification and control of physiological conditions; however, the goal of replicating physiologic (and more specifically perioperative conditions and various ventilation modalities) has proven to be difficult. Tangentially, *ex vivo* lung perfusion (EVLP) protocols have been developed as a technique to evaluate and recondition lungs prior to transplantation [20] and may provide an interesting extension to improved *ex vivo* lung models. During EVLP, lung function is monitored in real time including dO_2, dCO_2, glucose, and other parameters [20]–[22], which provides quantitative assessment of cellular health and overall tissue function. Despite a high degree of sophistication, current EVLP systems do not attempt to mimic the physiology of the pleural cavity. Instead, the lung is exposed to air and ventilated using positive pressure. Nevertheless, EVLP provides tremendous proof of principle showing that lungs can be ventilated and perfused *ex vivo* for several hours to observe physiologic function, assess tissue health, and (to a certain extent) repair damage in both porcine and human lungs [23].

To further expand the concept of EVLP and create a more prescriptive lung model to investigate PALs, a novel platform with *ex vivo* perfusion and ventilation was designed and built to enable the study of healthy porcine and diseased human lungs. In the present study, the overall goals of system design, equipment validation, and leak testing feasibility are presented along with data that aims to establish this novel model as a viable test method for future PAL studies.

II. Methods

A. System Design

To enable the clinically-relevant investigation of PAL etiology, a closed, isolated lung perfusion and ventilation system was developed to simulate *in vivo* lung mechanics and physiology of large animal and human lungs (Fig. 1). A focus of the effort was to assess the impact of simulated surgical procedures across intra- and post-operative phases with the capability to maintain lung function. Critical to the design was the ability to directly visualize the lungs, capture and quantify lung air leaks, perform both mechanical (positive pressure) and physiologic (negative pressure) ventilation, and simulate coughing.

The system (schematic shown in Fig. 1) consisted of a large (approximately 15 L) polycarbonate water-jacketed chamber with a 19 cm diameter piston [Fig. 1(a)] connected to the chamber bottom. A Cole-Parmer PolyStat recirculating water heater (Cole-Parmer, Vernon Hills, IL) controlled the temperature of the saline within the chamber via the water jacket. To mimic

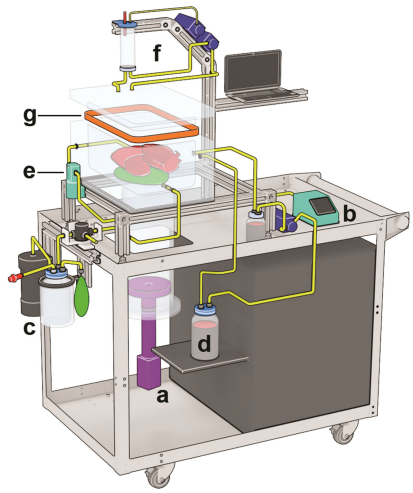

Fig. 1. Schematic of the *ex vivo* lung chamber consisting of: (a) piston and actuator enabled precise control of negative pressure ventilation, (b) clinical ventilator controlled positive pressure ventilation, (c) air compressor and PEEP valve maintained a set compliance in the chamber to mimic chest wall compliance and allow positive pressure ventilation, (d) perfusion circuit consisting of a heated reservoir, pulsatile pump, and dampening unit, (e) solenoid pinch valve for cough simulation, (f) leak quantification system including air collection cylinder, air removal pump, recirculation pump, and ultrasonic level sensor, and (g) custom EIT ring to measure ventilation.

diaphragmatic action, a single axis actuator and servo drive (Tolomatic, Hamel, MN) connected to the piston enabled a maximum volume change of 2750 ml in 1 ml increments across a wide range of rates (approximately 4–570 ml/sec); this allowed precise control of the tidal volume and respiratory rate of the lungs under negative pressure ventilation [Fig. 1(a)]. Positive pressure ventilation in the system was accomplished through an external clinical ventilator (Respironics Trilogy 200; Respironics, Murrysville, PA) [Fig. 1(b)] which was attached to the tracheal cannulation port. Balloons were positioned in the bottom of the lung chamber to simulate chest compliance and allow lung expansion during positive pressure ventilation in the closed system (closed lid). An air compressor and positive end expiratory pressure (PEEP) valve [Fig. 1(c)] maintained a set pressure within the compliance balloons; since the balloon pressures were adjustable, various clinical scenarios such as post-resection pleural spaces, pneumothoraxes, and pathological chest compliance changes could be simulated.

To perform pulsatile perfusion of the lungs, a perfusion circuit [Fig. 1(d)] consisting of a heated media reservoir and pulse damping chamber was built. Commercial luer fitting pressure transducers (PRESS-S-000; PendoTech, Princeton, NJ) were connected to the pulmonary artery (PA) and left atrium (LA) ports. A Masterflex L/S peristaltic pump (Cole-Parmer, Vernon Hills, IL) permitted pressure- and volume-controlled perfusion. Easy access to perfusate samples at PA and LA sites was necessary to assess lung function and viability through testing. Custom plastic cannulas with quick connect fittings were used to cannulate the PA above the pulmonary valve (inflow), the LA through the mitral valve annulus (outflow), and the trachea (ventilation) [Fig. 2(a)]. A pressure transducer and pneumotach

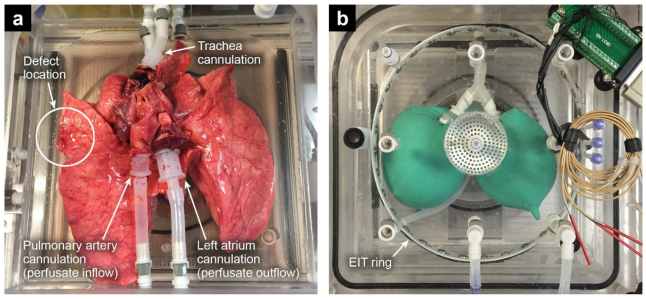

Fig. 2. (a) Representative lung set showing PA and LA cannulation for perfusion, tracheal cannulation for ventilation, and approximate location of induced defect; (b) EIT ring location within the chamber–note inflated compliance balloons.

(Biopac Systems, San Diego, CA) were connected to the trachea port to collect pressure and air flow data. Volume was computed by integrating the flow signal in 1 ms intervals, as performed in standard clinical spirometry tests [24], [25]. To simulate coughing, the trachea tubing was passed through a pinch valve solenoid (EPK-1502-NO; Takasago Electric, Nagoya, Japan) [Fig. 1(e)] which replicated the epiglottis to enable simulation of coughing or laryngospasm.

To accurately assess air leak volumes and rates in the closed system, a real-time leak quantification system was developed that separated, removed, and measured air volume from the chamber fluid; this system was necessary to prevent pneumothorax and lung collapse conditions in the presence of air leaks. A custom domed-lid was fabricated with recirculation ports placed at the peak of the dome (intake) and midway point (return). A Masterflex peristaltic pump cycled chamber fluid into a smaller, closed cylindrical chamber [Fig. 1(f)], and recirculated fluid passively drained back into the main chamber. Collected air separated from the fluid by rising to the top of the secondary chamber. An ultrasonic level sensor (UM12; Sick, Minneapolis, MN) was used to monitor the fluid level in the secondary chamber; if it fell outside of a user-defined set point (because of air accumulation in the secondary chamber), a Masterflex peristaltic pump would cycle on to remove air, returning the fluid level to the set point. Measuring the air removal pump speed permitted calculation of air volume removed.

Similar to systems used in clinical and research settings to measure lung ventilation [26]–[29] and organ perfusion [26]–[33], real-time imaging of air distribution in the lungs was enabled through a custom-designed electrical impedance tomography (EIT) array [Fig. 1(g)] and commercially available controller and software package (Swisstom; Landquart, Switzerland). A circular array of thirty-two electrodes was constructed to fit around the chamber [Fig. 2(b)] which provided a 2D slide of air distribution within the lungs. An open-source reconstruction algorithm (EIDORS; EIDORS3d.sourceforge.net) implemented within Matlab (Mathworks; Natick, MA) was used to analyze the array data.

To coordinate the functions of the various subsystems, a LabVIEW-based software program (National Instruments; Austin, TX) was developed to communicate with pumps, pressure sensors, piston, pneumotach, solenoid valve, and all other components. This enabled essential coordination of component functions, necessary to maintain macroscale physiological parameters. Although parameters (e.g., pump speed, cough pressures, respiratory rate, etc.) could be adjusted manually by the user, the software automatically maintained user-defined parameters during operation. Within LabVIEW, a PID controller maintained the leak collection chamber height, cycling on when required to remove accumulated air. The software also automatically collected and logged each data point at a user defined rate up to 20 Hz to produce a highly-detailed report of testing protocols with resolution down to individual breath cycles. Due to the complexities of switching between ventilation modalities, changing operation between mechanical ventilation and physiologic ventilation required user direction to manually turn off the ventilator and begin piston motion. Once settings were confirmed by the user, the software automatically controlled piston motion, leak collection, and data logging.

TABLE I
DESCRIPTION OF VENTILATION PHASES CONDUCTED IN THE *Ex Vivo* MODEL

	Peri-Operative Phase	Duration	Chest Compliance (Y/N)?	Ventilator Settings	Piston Settings
Full Positive Pressure	Open Chest	10 Minutes	YES	VC=800ml, PEEP=3 cm H20, Rate=10 br/min	Off
	Closing Chest	< 5 Minutes	YES	VC=800ml, PEEP=3 cm H20, Rate=10 br/min	Off
	Closed Chest	10 Minutes	YES	VC=800ml, PEEP=3 cm H20, Rate=10 br/min	Off
Mix of Positive and Negative Pressure	Reversal of Paralytics	10 Minutes	YES	VC=800ml, PEEP=3 cm H20, Rate=10 br/min	VC=150ml, Rate=5 br/min
	Emergence	10 Minutes	YES	SMIV PIP=25 cm H20, PEEP=5 cm H20, Rate=10 br/min	VC=400ml, Rate=10 br/min
	Spontaneous Ventilation	10 Minutes	YES	SMIV PIP=25 cm H20, PEEP=5 cm H20, Rate=10 br/min	VC=800ml, Rate=10 br/min
Full Negative Pressure	Post-Extubation	15 Minutes	NO	CPAP=5 cm H20	VC=800ml, Rate=10 br/min
	Coughing	5 Minutes	NO	CPAP=5 cm H20, 5 cough/min	VC=800ml, Rate=10 br/min
	Deep Breath	5 Minutes	NO	CPAP=5 cm H20	VC=1200ml, Rate=10 br/min

Note That VC = Volume Control Mode, SIMV = Synchronized Intermittent-Mandatory Ventilation, and CPAP = Constant Positive Airway Pressure.

B. Validation of Leak Measurement System

The accuracy of the air leak quantification system was assessed with a leak removal test of $n = 18$ trials, conducted using a 600 ml calibration syringe (Biopac; San Diego, CA) to inject a bolus of air which was subsequently cycled into the leak chamber, removed, and quantified over an average duration of 36 seconds. Since air delivery rates were variable for each trial, each dataset was normalized by time and leak volumes at regular normalized intervals (0, 0.1, 0.2, etc.) were averaged.

C. Leak Assessment Protocol

A protocol was designed to serve as a baseline testing routine to mimic clinical procedures. Porcine lungs were taken though a simulated perioperative procedure over the course of eighty minutes, with phases shown in Table I. Lungs were run under volume control either using the ventilator (positive pressure) or piston (negative pressure). Pressure-controlled synchronous intermittent-mandatory ventilation (SIMV) was employed during the transition from full positive to full negative ventilation

(Table I). Specific test phases lasted for ten minutes, except for coughing and deep breathing which were shortened to five minutes due to their clinically transient nature. The duration of the chest closing phase was variable in length due to lid closing and excess air purging but lasted approximately five minutes. Leak rate was measured throughout the duration of the simulated procedure. Trachea flow rate, trachea volume, air leak rate, tissue temperature, perfusate temperature, trans-pulmonary pressure, chamber pressure, tracheal pressure, arterial and venous perfusion pressure, and vascular resistance (during perfusion) were collected at 20 Hz during testing.

Nine porcine heart-lung blocs (Midwest Research Swine; Gibbon, MN) from 110–120 kg pigs were harvested within fifteen minutes of euthanasia, flushed antegrade with heparinized saline through the right atrium, and shipped overnight on wet ice for testing in the system. Cannulas were attached to the PA and LA with umbilical tape [Fig. 2(a)] and deaired using an in-house formulated perfusate similar to commercially available Perfadex [34]. The trachea cannula was attached with umbilical tape proximal to the cranial lobe airway bifurcation [Fig. 2(a)]. Lungs were slowly warmed in a water bath and were gently inflated using an Ambu bag attached to the tracheal cannula until the lungs were recruited. Upon recruitment, a 0.5 mm deep defect was created in the right cranial lobes of each lung using a 20-gauge needle, resulting in an approximate leak of 100–250 ml/min [Fig. 2(a)]. Lungs were placed in a partially-filled chamber with saline maintained at 37 °C. With the chamber lid open, testing progressed for ten minutes in an open chest/mechanical ventilation phase. An approximately five-minute chamber closing phase (simulating surgical closure of the chest) was conducted, followed by a ten-minute closed chest/mechanical ventilation phase. Emergence from paralysis/anesthesia (shallow negative pressure ventilation with full mechanical support) and spontaneous ventilation (full negative pressure ventilation with full mechanical support) were simulated for ten minutes each, while post-extubation (full negative pressure ventilation with no mechanical support) was simulated for fifteen minutes. A five-minute intermittent coughing phase (5 coughs/min) was then simulated, followed by a five-minute deep breathing phase (150% baseline volume). Because of the potential for variability in leak rates between specimens, a normalized value (x_{norm}) was computed based on the maximum ($x_{\max}$) and minimum ($x_{\min}$) leak rate values for a given specimen, as described by:

$$x_{\mathrm{norm}} = \frac{(x - x_{\min})}{(x_{\max} - x_{\min})} \tag{1}$$

where $x_{\max}$ and $x_{\min}$ were found for each specimen across the entire testing protocol (these maximum and minimum values represent the maximum and minimum across all testing phases for each tested lung).

D. EIT and Perfusion

Using EIT, ventilation was monitored during testing to ensure adequate air ventilation, especially in the right cranial lobe (site of defect). Impedance data was recorded at 10 frames/sec and imported into the EIDORS software. Approximately 10 respiratory cycles were cropped from the entire data file to facilitate single-cycle analysis. Using a masking tool within Matlab, right and left lung boundaries were hand-selected from a peak impedance map from a given cycle. Single cycle impedance waveforms, right and left like quadrant impedance waveforms, and peak impedance (represented as % of tidal volume) were outputted. Perfusion was maintained at 250 ml/min with a 1 Hz sinusoidal waveform to simulate cardiac output. Perfusate baseline sample and LA outflow samples at five, ten, and fifteen-minute intervals were collected from six lungs to monitor electrolytes and blood gasses such as pCO_2, pO_2, and pH, as well as glucose. An i-STAT handheld blood analyzer (Abbott, Illinois USA) and CG8+ cartridges (general blood gas panel analysis including glucose, pH, pCO_2, pO_2, and $HC0_3$) were utilized to perform the analysis.

Preparation of the lungs required approximately sixty minutes per lung set. Individual tests lasted approximately eighty minutes. The addition of perfusion and EIT imaging increased testing and setup time by sixty minutes. With multiple tests performed in series, it was possible to complete approximately four tests per day.

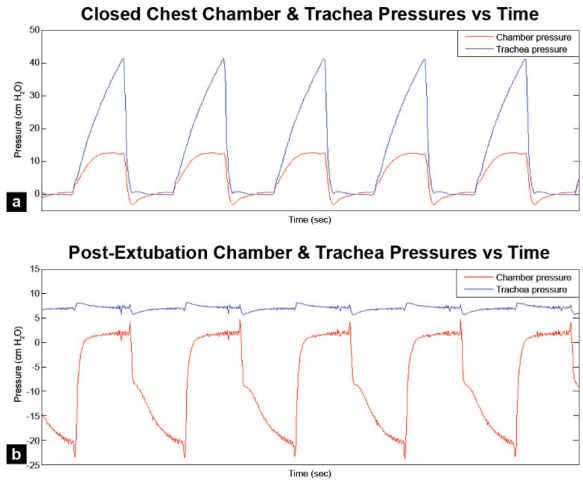

Fig. 3. Representative plots of tracheal and chamber pressures versus time, with (a) collected during the closed chest phase (positive pressure ventilation) and (b) collected during the post-extubation phase (negative pressure ventilation).

III. Results

A. Comparison to Clinical Data

Ventilation flow, volume, and pressure were continuously recorded through all phases in the tested lungs. Representative pressure data points from the trachea, chamber (pleural space), PA, LA, and chest compliance balloons were plotted over the course of multiple breath cycles for closed chest (positive pressure ventilation) and post-extubation (negative pressure ventilation) phases, as shown in Fig. 3(a) and (b). Cycles from positive pressure (closed chest, full mechanical ventilation) and negative pressure (post extubation) phases were averaged for each tested lung.

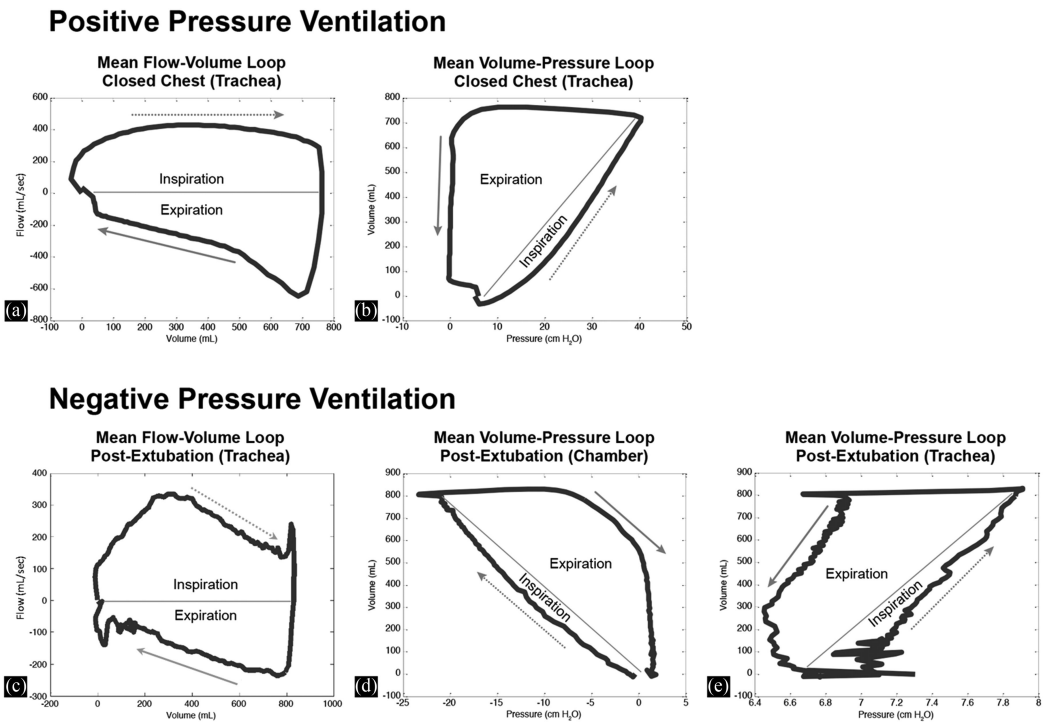

Fig. 4. Positive pressure (closed chest) phase (a) mean flow-volume loop and (b) mean volume-pressure loop, with pressure measured at the tracheal port. Negative pressure (post-extubation) phase (c) mean flow-volume loop and (d) mean volume-pressure loop, with pressure measured at the chamber port. Negative pressure phase (e) mean volume-pressure loop, with pressure measured at the tracheal port. In all subplots, volume was computed from flow measured at the tracheal port. Lines and labels indicate inspiration and expiration portions of the loops, and arrows indicate direction along the loops.

TABLE II
SUMMARY OF MEANS AND STANDARD DEVIATIONS OF MAXIMUM INSPIRATORY VOLUME, TRACHEA PRESSURE, AND LEAK RATE FROM POSITIVE PRESSURE (CLOSED CHEST) AND NEGATIVE PRESSURE (POST-EXTUBATION) VENTILATION FROM EACH TESTED LUNG

		Lung01	Lung02	Lung03	Lung04	Lung05	Lung06	Lung07	Lung08	Lung09	Mean +/- Pooled Std. Dev.
Positive Pressure Ventilation	Max Inspiratory Volume (ml)	694 +/- 190	477 +/- 222	522 +/- 62.4	767 +/- 29.7	781 +/- 32.2	477 +/- 41.2	587 +/- 46.5	516 +/- 48.7	548 +/- 37.2	**597 +/- 105**
	Max Trachea Pressure (cm H20)	40.3 +/- 2.15	37.8 +/- 0.243	41.2 +/- 0.328	40.6 +/- 0.705	39.8 +/- 0.104	36.3 +/- 0.219	30.4 +/- 0.238	41.0 +/- 0.190	48.9 +/- 0.555	**39.6 +/- 0.799**
	Leak Rate (ml/min)	80.1 +/- 8.59	73.4 +/- 3.20	109 +/- 25.1	19.1 +/- 7.52	153 +/- 9.69	133 +/- 9.55	77.1 +/- 6.30	45.7 +/- 6.41	116 +/- 7.07	**89.5 +/- 11.0**
Negative Pressure Ventilation	Max Inspiratory Volume (ml)	718 +/- 291	617 +/- 347	605 +/- 163	812 +/- 114	495 +/- 219	511 +/- 68.0	681 +/- 94.6	708 +/- 79.6	633 +/- 77.7	**642 +/- 188**
	Max Trachea Pressure (cm H20)	2.40 +/- 0.241	13.1 +/- 1.32	1.26 +/- 0.419	7.32 +/- 1.38	9.40 +/- 0.536	8.66 +/- 0.352	1.08 +/- 0.968	7.28 +/- 0.809	16.1 +/- 0.625	**7.41 +/- 0.835**
	Min Chamber Pressure (cm H20)	-19.4 +/- 2.94	-18.4 +/- 4.10	-14.1 +/- 2.54	-18.4 +/- 4.26	-9.02 +/- 0.81	-26.4 +/- 1.16	-15.4 +/- 3.89	-19.9 +/- 0.90	-18.8 +/- 2.42	**-17.8 +/- 2.86**
	Leak Rate (ml/min)	324 +/- 55.0	205 +/- 8.55	1180 +/- 107	95.8 +/- 6.31	350 +/- 23.8	1100 +/- 30.1	72.2 +/- 31.7	210 +/- 45.8	360 +/- 31.5	**433 +/- 47.2**

Minimum Chamber Pressures From Negative Pressure Ventilation are Also Provided. Mean +/− Standard Deviation is From All Cycles Within a Given Testing Phase. Means and Pooled Standards Deviation From All Nine Animals Are Provided in the Rightmost Column.

Fig. 4(a) and (b) displays mean flow-volume and mean pressure-volume loops, respectively, under positive pressure ventilation (closed chest phase). Pressure and flow were measured at the tracheal port. Fig. 4(c) and (d) displays similar data under negative pressure ventilation (post-extubation phase), except with pressure measured at the chamber port (flow measured at the tracheal port). Fig. 4(e) shows mean pressure-volume under negative pressure, but with the pressure measured at the tracheal port. Table II summarizes mean maximum tracheal pressures (positive pressure), mean

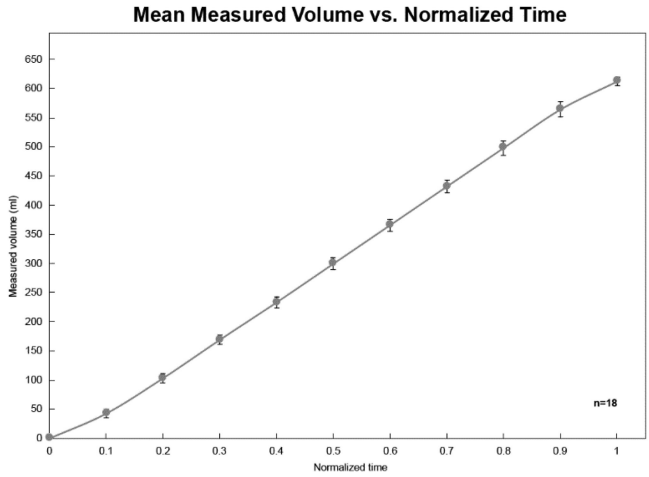

Fig. 5. Leak validation data from $n = 18$ air injections (600 ml each) into the saline-filled chamber, showing mean +/− standard deviation of the measured volume (ml) versus normalized time. Measured volumes deviated minimally from the actual injected volumes through most of the test, with the greatest discrepancies (+/−6.5% of injected volume) observed at the start and end of the test.

minimum chamber pressures (negative pressure), and maximum lung volumes (based on trachea pressure) for each tested lung as well as pooled values for all lungs.

B. Leak System Validation and Air Leak Testing

Mean +/− standard deviation of leak volume (ml) versus normalized time for the 18 syringe validation trials is shown in Fig. 5. Volumes were accurate to within ±6.5 ml or ∼1% at each normalized time. Air leak data for each ventilation phase and from each lung set was collected and plotted as a box and whisker plot of average normalized leak rate (%) over the course of the testing phases (Fig. 6); in this plot, boxes represent the first to third quartiles of data with solid lines in the boxes representing median values. Whiskers extend out to the minimum and maximum values. Closed chest showed an average normalized leak rate (7.66% +/−6.46%), with leak rate gradually increasing through reversal, emergence, and spontaneous (negative pressure with full mechanical support) phases. A sharp increase was observed between spontaneous (24.7% +/−11.1%) and post-extubation phases (63.3% +/−20.0%), which marked the onset of full negative-only pressure ventilation. Coughing and deep breathing phases had minimal impact on leak rate. Perfusing the lungs (averaged for $n = 3$ specimens) decreased the leak rate (36.8% +/−12.2%) from post-extubation slightly, but it was still larger than the positive pressure phases.

C. Air Distribution and Perfusion

A representative analysis of EIT data is shown in Fig. 7. Peak impedance [Fig. 7(a)] within the EIT ring fit that of the lung set outline. Right/left lung set distribution was similar [Fig. 7(b)], with the right lung having a slightly larger tidal volume as shown in other studies on lung volume distribution [35], and with further distinction into quadrants showing similar tidal volume distributions in the cranial and caudal regions. Differences in the central quadrants were evident but may have resulted from the presence of the accessory lobe (right lung) in the lower central quadrant. Individual quadrant impedance versus time [Fig. 7(c)] and total impedance change versus time [Fig. 7(d)] displayed regular patterns that followed the prescribed volume versus time waveform of the system.

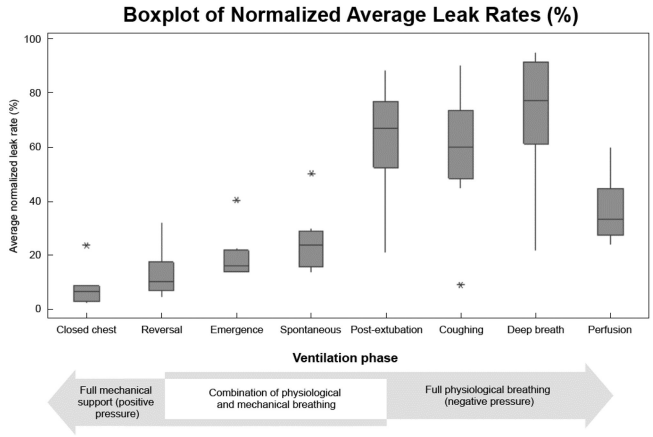

Fig. 6. Box and whisker plot showing the normalized average leak rate (%) versus ventilation phase from all tested lung sets. Boxes denote the first to third quartiles of the data, lines within the boxes represent the mean of the data, and the whiskers extend to the maximum and minimum data values. Asterisks indicate outliers (defined in Minitab as at least 1.5 time the interquartile range from the box edge). Note that as negative pressure ventilation is introduced (reversal, emergence, spontaneous), leak rate increases above that during full positive pressure (closed chest phase). Upon switching to full negative pressure (post-extubation), the average leak rate substantially increases and is maintained during coughing, deep breath, and perfusion phases.

TABLE III
SUMMARY PERFUSATE ANALYSIS FROM PERFUSED LUNGS

	0 min	5 min			10 min			15 min		
		Mean	Std. Dev.	N	Mean	Std. Dev.	N	Mean	Std. Dev.	N
pH	7.40	7.04	0.193	4	6.90	0.183	5	6.83	0.165	6
pCO2 (mm Hg)	7.4	9.9	1.3	4	10.4	1.5	5	10.4	0.95	6
PO2 (mm Hg)	153	132	7.02	4	125	16.5	5	129	17.4	6
BE (mmol/L)	-9	< -30	NA	4	< -30	NA	5	< -30	NA	6
HCO3 (mmol/L)	10.3	2.8	0.98	4	2.1	0.74	5	1.8	0.62	6
sO2 (%)	100	97	1.6	4	94	3.3	5	94	3.5	6
Na(mmol/L)	145	144	6.03	4	145	5.69	5	148	7.26	6
K (mmol/L)	7.7	7.8	0.42	4	7.9	0.35	5	7.6	0.37	6
iCa (mmol/L)	< 0.25	< 0.25	NA	4	< 0.25	NA	5	< 0.25	NA	6
Glucose (mg/dl)	92	65	8.2	3	67	1.5	3	68	5.6	4

Baseline (0 min) Data From Single Sample Analysis of Perfusate Before Circulating in Lungs. Perfusate samples Taken From LA pressure Transducer Port.
BE Denotes Base Excess, iCa Denotes Ionized Calcium, and sO2 Represents Oxygen Saturation.

Summary data from the perfusate analysis are presented in Table III. A total of six lung sets were perfused, though not all electrolytes/blood gasses were measured by the i-stat device at each time interval; therefore, the number of samples used to compute the mean and standard deviation are presented as well. Mean +/− standard deviation of pH, pCO_2, pO_2, and HCO_3 are shown in Fig. 8. Throughout ventilation, pO_2 was maintained at 125–132 mm Hg under room air. $PC0_2$ increased throughout perfusion from 7.4 to 10.4 mm Hg while pH dropped from 7.40 to 6.83. Glucose decreased from 92 mg/dl (baseline) to 65–68 mg/dl during ventilation. Bicarbonate ion concentration (HCO_3) dropped from 10.3 mmol/L (baseline) to 2.8 mmol/L

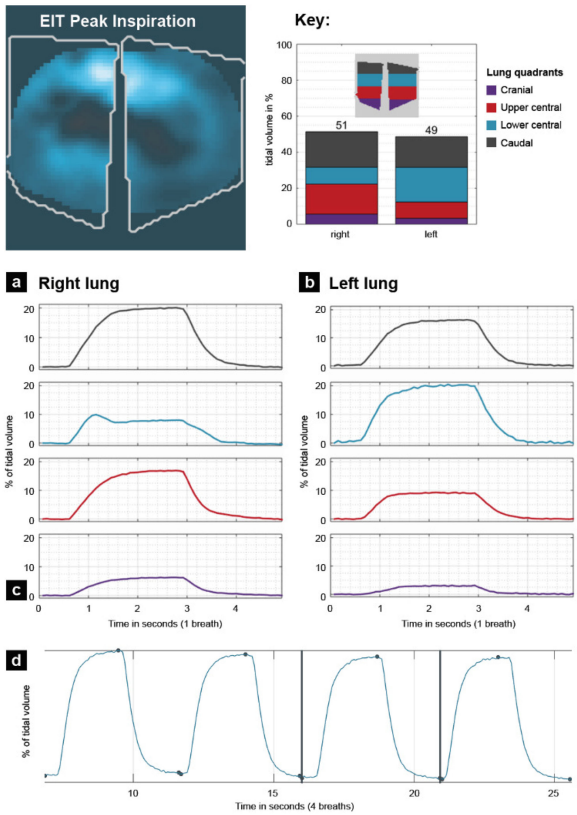

Fig. 7. Electrical Impedance Tomography analysis from a representative set of lungs: (a) shows EIT image from peak inspiration of a single cycle, with rough outline of the lungs shown in white, while (b) shows distribution of tidal volume percentage between right and left lungs with colored bars representing tidal volume percentage from quadrants of each lung. In (c), tidal volume percentage vs. time is plotted for each quadrant from both sides; note the similar distribution in tidal volume percentage between right and left lungs in the caudal and cranial quadrants. The difference between distributions in the central quadrants could be due to the location of the heart (lowering impedance) and the presence of the accessory lobe. In (d), tidal volume for the entire lung set vs. time is presented for four cycles.

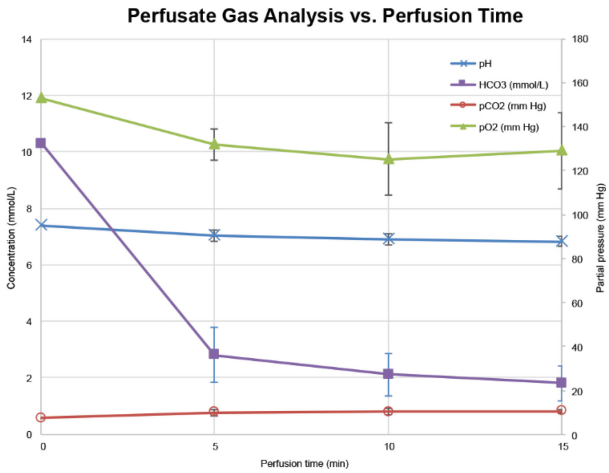

Fig. 8. Plot of perfusate gas analysis versus perfusion time, showing mean +/− standard deviation of pH, HCO3, pCO2, and pO2. During initial perfusion, pH, pO2, and pCO2 dropped–the drop in pH is suggestive of acidosis, with the drop in HCO3 suggestive of a metabolic cause. Glucose data (shown in Table III) supports metabolic acidosis. Through continued perfusion, pO2 stabilized and remained above 93% saturation.

and then steadily decreased to 1.8 mmol/L. Sodium and potassium ions did not substantially change from baseline.

IV. Discussion

A. Model Design

The primary endpoint of this current work was to develop and validate a novel clinically-relevant and physiologically-based thoracic model to explore PAL etiology, with the long-term goal of using the model to help develop new and innovative solutions to reduce or prevent air leaks in thoracic surgery. To this end, this work demonstrates a completion of the primary endpoint and a significant step towards the long-term goal. Key design criteria such as the ability to simulate various ventilation modalities (full mechanical/positive pressure, assisted mechanical, full physiological breathing/negative pressure), accommodate visualization of the lungs, quantify and categorize air leaks, and maintain tissue function/viability were achieved. The various subsystems of perfusion, gas exchange monitoring, and lung imaging with EIT–along with the means to assess various ventilation modalities–enable users to scale the complexity of experiments based on specific variables of interest. As such, single specimen tests can be completed in less than an hour or can last multiple hours, depending on the desired experiment design.

As shown in the summary table, tracheal and chamber pressures were consistent among the $n = 9$ tested lungs as evidenced by the small standard deviations. Maximum inspiratory volumes were somewhat more varied, both within a lung and across lungs. Since these tests were run under a pressure-limited volume control mode, inspiration may have stopped prior to the volume set point if the pressure limit was reached (40 cm H20 pressure); therefore, some variations in volume could have resulted. Additionally, the presence of leak (especially under negative pressure) could have influenced maximum inspiratory volumes, and normal animal-animal variations could have contributed to the volume differences between individual lungs. Overall, considering the sources of variation, the standard deviations in lung volumes were low. Minimum chamber pressure (negative pressure) and leak rate were consistent within each lung and among all tested lungs.

In the air leak quantification system validation, a slight underestimation/overestimation was observed within the first and last ∼4 seconds of the test, likely due to the selected gain constant in the ultrasonic sensor by which the removal pump was activated (to return the fluid level back the set point). Overall, the discrepancies from anticipated values were exceptionally small, which built confidence in the leak collection and quantification system.

B. Comparison to Published Models

A survey of the current literature involving *ex vivo* lung models [11]–[17] highlights the unique advances in this current model, especially in the capacity to mimic various breathing modalities in intra- and post-operative settings and in the ability to capture and quantify air leaks. The system represents a

step beyond previous models of negative pressure ventilation of isolated lungs [17], [18] by employing a submerged lung model with controlled volumetric expansion of the chamber to expand the lungs as opposed to application of a pressure gradient to induce a volume change. By using volume change to induce negative pressure, the system provides control over both respiratory rate and tidal volume simultaneously, allowing for highly controlled physiologic breathing mechanics. Submerged lung models have been reported in rodent models [17]; however, the ventilation rates and conditions were non-physiologic, and the reported models did not replicate clinical interventions or provide leak quantification.

C. Clinical Representation

Mean flow-volume (QV) loops were produced that exhibited the same general progression of ventilation conditions as in clinical volume-controlled mechanical ventilation and patient spirometry curves [36]. Like typical QV loops under mechanical ventilation, a sharp increase in flow followed by a plateau was observed during inspiration. A sharp decrease in flow with a gradual return to zero marked expiration. Inspiration rates were slightly smaller than expiration rates, which is typical under normal airway resistance [36]. In the QV loops under negative pressure ventilation, a sharp increase in flow at the beginning of inhalation followed by a gradual tapering as peak tidal volume was achieved, similar to normal breathing spirometry curves. Some flow restriction was observed in the ventilation system, as shown by a slight blunting of the QV spirometry curves. This was likely created by the tracheal cannulation, pneumotach, solenoid, and tubing; similarly, intubated patients also face flow restrictions not dissimilar to that shown in the current model [36].

The pressure-volume (PV) loops under mechanical ventilation had similar features to clinical patient loops, with a broad increase in pressure towards peak volume [36]. Note in these experiments, a PEEP of $\sim$5–7 cm H_20 was maintained, and the volume control ventilation mode (set to 800 ml volume) had a pressure limit of 40 cm H_20. Upon expiration, the curve exhibited minimal change in volume with pressure decrease, which implied an increased in compliance. The lung defect may have contributed to the changes in the shape of the expiration curve. Since each of the lungs leaked, inspired air volume may have preferentially exited the leak site during the onset of expiration until sufficiently lower trachea pressure drew the remaining volume out of the trachea.

Under negative pressure ventilation, the trachea PV loop showed the tidal volume change with minimal change in pressure, as expected with naturally breathing lungs with a small CPAP applied [36]. Sharp changes in pressure at the onset of inspiration and expiration of the negative pressure trachea PV loop were likely caused by the ventilator attempting to maintain the CPAP setpoint during filling and emptying of the lungs. Negative pressure PV loops which approximated intrapleural pressure with chamber pressure displayed a similar pattern as in positive pressure ventilation, with a steady increase in volume with pressure change (negative in this case) upon inspiration and a more rapid decrease in volume with pressure increasing back to zero. Again, increased compliance and the presence of air leaks could have contributed to the shape of the PV curve.

D. Leak Assessment

Intentionally introducing a defect in the lungs to induce an air leak and monitoring leak through various simulated intra- and post-operative breathing phases gave rise to surprising leak rate results. Marginal increases in leak rate were observed as the ventilation mode changed from full mechanical support (positive pressure) towards spontaneous breathing (intermittent positive pressure with full negative pressure ventilation). Interestingly, a sharp rise in leak rate was evident in the post-extubation phase (full negative pressure breathing). This transition between positive and negative pressure ventilation appears to represent a critical factor in determining the magnitude of the leak rate. The larger whiskers on the post-extubation and coughing phases were caused by a single specimen that had lower leak rates throughout testing (in the coughing phase, it was sufficiently low to be removed as an outlier). Despite one specimen showing lower rates, the trend was apparent in the other eight tested lung sets. Further stressing of the lungs (cough, deep breath) did not have a significant impact on leak rate. In his publication describing an air leak rating system, Cerfolio, states that all forced expiratory leaks (those revealed under coughing only) are smaller than expiratory air leaks (leaks revealed under expiration only) [37]. Likewise, he states that expiratory leaks are smaller than inspiratory leaks [37]. Our observations are consistent with his description. It is possible that the addition of coughing or deep breathing with an existing expiratory/inspiratory leak was not substantially larger than expiratory/inspiratory leaks alone.

The underlying mechanism driving the apparent marked difference in leak rate between positive and negative pressure ventilation will likely be an important topic of further exploration in future tests with this *ex vivo* lung system. One hypothesis as to the cause of the observed difference is that the pressure modalities are fundamentally different in how they interact with tissue. In the case of positive pressure, air is being forced into the large airways, overcoming increasing airway resistance to reach the alveoli. When alveolar pressure exceeds that of the pleural pressure (and overcomes tissue elasticity), the lungs inflate. Under negative pressure, the entire pleural surface of the lung is being acted upon, with the pressure pulling the lung open. As pleural pressure drops below alveolar pressure, the pressure gradient acts to pull the lungs open. Since such forces directly influence tissue deformation, existing lung damage/holes may be more susceptible to stretching open under negative versus positive pressure. As observed in the PV curves in this study, a much larger pressure gradient was generated during positive pressure ventilation (approximately 40 cm H_2O) compared to negative pressure (approximately -18 cm H_2O) with comparable tidal volumes, suggesting that negative pressure ventilation is more efficient at inflating lung than positive pressure ventilation. Additionally, the mass effect of surrounding lung segments that may compress the leak during positive pressure ventilation may be reduced or removed during negative ventilation, thereby worsening the leak.

E. Air Distribution and Perfusion

Despite a number of advances in medical imaging of lungs including xenon-gas contrast enhanced CT [38], [39], hyperpolarized xenon or helium gas enhanced MRI scans [40], [41], and various advanced segmentation techniques [42], [43], design constraints necessary to enable critical system capabilities in the current model led to the selection of EIT as a suitable means to evaluate gas distribution within the lungs during ventilation. EIT proved successful in identifying ventilation of the entire lung as well as comparison of ventilation within the sides and regions (quadrants of each side) of the lung. Overall, the data suggests that the lungs ventilated equally between sides, with high impedances (indicative of ventilation) observed in the region near the leak site. Impedance curves followed that of the tracheal pressure curves. Areas of low impedance (notably the center of the ring) matched with the approximate location of the heart (which would have a lower impedance than air).

Results of the perfusate analysis are consistent with published data on glucose metabolism, indicating organ viability [44]. The observed mild acidosis and electrolyte changes match that of tissue perfusion and ischemia reperfusion injury in lungs with cold ischemia time of 24 hours and longer. Measured LA (pulmonary venous) oxygen and carbon dioxide partial pressures are representative of tissue ventilation and perfusion and are similar to prior data on prolonged isolated lung culture [45]–important observations to drive towards functional lungs in the model.

F. Limitations and Future Work

Although designed to better replicate physiological function, the current model is not without limitations. The evaluation of air leaks utilized lungs from young, healthy pigs which likely does not mimic the surgical patient population. Nevertheless, it was appropriate to evaluate the system with a tissue source with as little heterogeneity as possible (i.e., without disease) to better assess the functionality of the system. Testing was limited to an acute, eighty-minute time frame; as PALs often manifest 1–2 days after surgery, there may be critical changes in leak rates that were not observed in the current testing. Finally, although the use of a saline bath was essential to capture and quantify leaks, the addition of a hydrostatic pressure on the lungs may have induced non-physiologic deformations. This risk was mitigated by limiting leaks to the ventral surface of the lungs which resided near the top of the chamber, greatly minimizing the hydrostatic head at the leak site and therefore variation between test samples.

Future work will focus on replicating leaks from lung resection procedures associated with tissue handling as well as with stapling devices to evaluate resulting leaks under the different pressure modalities. Additionally, the potential to use transplant-rejected human tissue with pathological states clinically representative of patients would greatly deepen understanding of the science around leak etiology, specifically as it applies to the surgical arena. Finally, lengthening the testing phase to better approach post-operative periods where PALs manifest (up to two days), may add novel insights into how leaks change over clinically-relevant time periods. These efforts are aimed at extending the pressure modality dependency on leaks observed in the current study to conditions that better mimic the clinic, furthering the clinical translation of the model. Ultimately, the ability to mitigate or eliminate the risk of air leaks through novel surgical devices or peri-operative management strategies compels further usage of this model to address the unmet need of PALs.

V. Conclusion

This work represents a significant step forward in understanding a current challenge in thoracic surgery: prolonged air leaks. A novel *ex vivo* lung model was designed and constructed to better replicate *in vivo* conditions, with an emphasis placed on mimicking physiological breathing (negative pressure) and organ perfusion. A leak collection and quantification system was developed and validated to enable the study of air leak etiology and evolution through various ventilation modalities. Preliminary exploratory work using porcine lungs demonstrated basic chamber functionality (ventilation, perfusion, gas exchange) and revealed surprising differences in leak rates based on positive and negative pressure ventilation modes. Importantly, this work serves as the foundation for future studies to understand leak etiology in diseased tissue and how current and future surgical techniques and devices influence air leaks.

Acknowledgment

The authors would like to thank D'Van Howard for his artistic contributions in creating the system schematic. Both H. C. Ott and L. J. Wudel serve as paid consultants for Ethicon, Inc, a Johnson & Johnson Company. Authors had full access to all data, devices, and materials utilized in the study and take complete responsibility for the integrity of the data and the accuracy of the data analysis and interpretations of outcomes. Cadaveric animal tissue was procured from Midwest Research Swine (Gibbon, MN) which is licensed by the US Department of Agriculture under the Animal Welfare Act. All work was conducted following ethical guidelines and according to internationally-accepted standards regarding animal welfare in permitted lab space maintained by Northshore Innoventures (Beverly, MA).

References

[1] S. Singhal *et al.*, "Management of alveolar air leaks after pulmonary resection," *Ann. Thorac. Surg.*, vol. 89, no. 4, pp. 1327–1335, Jun. 2010.
[2] A. Brunelli *et al.*, "Air leaks after lobectomy increase the risk of empyema but not of cardiopulmonary complications: A case-matched analysis," *Chest*, vol. 130, no. 4, pp. 1150–1156, Jul. 2006.
[3] G. Varela *et al.*, "Estimating hospital costs attributable to prolonged air leak in pulmonary lobectomy," *Eur. J. Cardiothorac Surg.*, vol. 27, no. 2, pp. 329–333, Feb. 2005.
[4] A. Yoo *et al.*, "Burden of air leak complications in thoracic surgery estimated using a national hospital billing database," *ClinicoEconomics Outcomes Res.*, vol. 9, pp. 373–383, 2017.
[5] R. J. Cerfolio *et al.*, "Predictors and treatment of persistent air leaks," *Ann. Thorac. Surg.*, vol. 73, no. 6, pp. 1727–1721, Jun. 2002.
[6] A. Abolhoda *et al.*, "Prolonged air leak following radical upper lobectomy: An analysis of incidence and possible risk factors," *Chest*, vol. 113, no. 6, pp. 1507–1510, Jun. 1998.

[7] R. J. Cerfolio *et al.*, "Prospective randomized trial compares suction versus water seal for air leaks," *Ann. Thorac. Surg.*, vol. 71, no. 5, pp. 1613–1617, May 2001.

[8] H. Elsayed *et al.*, "Air leaks following pulmonary resection for lung cancer: Is it a patient or surgeon related problem?," *Ann. Roy. Coll. Surg. Engl.*, vol. 94, no. 6, pp. 422–427, Sep. 2012.

[9] S. Okada *et al.*, "Prolonged air leak following lobectomy can be predicted in lung cancer patients," *Surg. Today*, vol. 47, no. 8, pp. 973–979, Aug. 2017.

[10] V. W. Rusch *et al.*, "The performance of four pleural drainage systems in an animal model of bronchopleural fistula," *Chest*, vol. 93, no. 4, pp. 859–863, Apr. 1988.

[11] L. S. Wang *et al.*, "The effect of ischemic time and temperature on lung preservation in a simple ex vivo rabbit model used for functional assessment," *J. Thorac. Cardiovasc. Surg.*, vol. 98, no. 3, pp. 333–342, Sep. 1989.

[12] A. Linder *et al.*, "The ex-vivo isolated, perfused human lung model: Description and potential applications," *Thorac. Cardiovasc. Surg.*, vol. 44, no. 3, pp. 140–146, Jun. 1996.

[13] P. Macchiarini *et al.*, "Ex vivo lung model of pig-to-human hyperacute xenograft rejection," *J. Thorac. Cardiovasc. Surg.*, vol. 114, no. 3, pp. 315–325, Sep. 1997.

[14] R. W. Niemeier, "The isolated perfused lung," *Environ. Health Perspectives*, vol. 56, pp. 35–41, Jun. 1984.

[15] H. C. Ott *et al.*, "Regeneration and orthotopic transplantation of a bioartificial lung," *Nat. Med.*, vol. 16, no. 8, pp. 927–933, 2010. [Online]. Available: http://www.nature.com/nm/journal/v16/n8/full/nm.2193.html?foxtrotcallback=true

[16] X. Ren *et al.*, "Engineering pulmonary vasculature in decellularized rat and human lungs," *Nat. Biotechnol.*, vol. 33, no. 10, pp. 1097–1102, Oct. 2015.

[17] K. Nelson *et al.*, "Method of isolated ex vivo lung perfusion in a rat model: Lessons learned from developing a rat EVLP program," *J. Vis. Experiments*, vol. 96, Feb. 2015.

[18] K. Nelson *et al.*, "Animal models of ex vivo lung perfusion as a platform for transplantation research," *World J. Exp. Med.*, vol. 4, no. 2, pp. 7–15, May 2014.

[19] T. H. Petersen *et al.*, "Bioreactor for the long-term culture of lung tissue," *Cell Transplant.*, vol. 20, no. 7, pp. 1117–1126, 2011.

[20] S. Steen *et al.*, "First human transplantation of a nonacceptable donor lung after reconditioning ex vivo," *Ann. Thorac. Surg.*, vol. 83, no. 6, pp. 2191–2194, Jun. 2007.

[21] C. Aigner *et al.*, "Clinical ex vivo lung perfusion–pushing the limits," *Amer. J. Transplant.*, vol. 12, no. 17, pp. 1839–1847, Jul. 2012.

[22] C. G. Curtis *et al.*, "Ex vivo metrics, a preclinical tool in new drug development," *J. Transl. Med.*, vol. 6, no. 5, Jan. 2008.

[23] M. Cypel *et al.*, "Normothermic ex vivo lung perfusion in clinical lung transplantation," *New Engl. J. Med.*, vol. 364, no. 15, pp. 1431–1440, Apr. 2011.

[24] R. Pierce, "Spirometry: An essential clinical measurement," *Aust. Family Physician*, vol. 34, no. 7, pp. 535–539, Jul. 2005.

[25] M. R. Miller *et al.*, "Standardisation of spirometry," *Eur. Respir J.*, vol. 26, no. 2, pp. 319–338, 2005.

[26] P. W. Kunst *et al.*, "Ventilation and perfusion imaging by electrical impedance tomography: A comparison with radionuclide scanning," *Physiol. Meas.*, vol. 19, no. 4, pp. 481–490, 1998, Nov.

[27] D. Holder, "Clinical and physiological applications of electrical Impedance tomography," *Thorax*, vol. 49, no. 6, pp. 626–626, Jun. 1994.

[28] B. Brown, "Electrical impedance tomography (EIT): A review," *J. Med. Eng. Technol.*, vol. 27, no. 3, pp. 97–108, 2003.

[29] A. Adler and R. Guardo, "Electrical impedance tomography: Regularized imaging and contrast detection," *IEEE Trans. Med. Imaging*, vol. 15, no. 2, pp. 170–179, 1996.

[30] J. B. Borges *et al.*, "Regional lung perfusion estimated by electrical impedance tomography in a piglet model of lung collapse," *J. Appl. Physiol.*, vol. 112, no. 1, pp. 225–236, Jan. 2012.

[31] D. T. Nguyen *et al.*, "Preliminary results on different Impedance contrast agents for pulmonary perfusion imaging with electrical Impedance tomography," in *Proc. J. Phys. Conf. Series*, 2013, vol. 434.

[32] I. Frerichs *et al.*, "Regional lung perfusion as determined by electrical impedance tomography in comparison with electron beam CT imaging," *IEEE Trans. Med. Imaging*, vol. 21, no. 6, pp. 646–652, Jun. 2002.

[33] Y. P. Mamatjan *et al.*, "Use of temperature as a contrast agent in electrical impedance tomography," in *Proc. Canadian Medical and Biological Engineering Society*, Ottawa, ON, Canada, May 2013.

[34] A. M. Padilla and J. D. Padilla, "Lung preservation: Current practices, *Arch. Bronconeumol.*, vol. 40, no. 2, pp. 86–93, Feb. 2004.

[35] N. Jahani *et al.*, "Assessment of regional ventilation and deformation using 4D-CT imaging for healthy human lungs during tidal breathing," *J. Appl. Physiol.*, vol. 119, no. 10, pp. 1064–1074, Nov. 2015.

[36] J. M. Cairo, "Burden of air leak complications in thoracic surgery estimated using a national hospital billing database," in *Pilbeam's Mechanical Ventilation: Physiological and Clinical Applications*, 6th ed. St. Louis, MO, USA: Elsevier, 2016.

[37] R. J. Cerfolio, "Advances in thoracostomy tube management," *Surg. Clin. North Amer.*, vol. 82, no. 4, pp. 833–848, Aug. 2002.

[38] E. J. Chae *et al.*, "Xenon ventilation CT with a dual-energy technique of dual-source CT: Initial experience," *Radiology*, vol. 248, no. 2, pp. 615–624, Aug. 2008.

[39] J. W. Jung *et al.*, "New insights into the assessment of asthma using xenon ventilation computed tomography," *Ann. Allergy Asthma Immunol.*, vol. 111, no. 2, pp. 90–95, Aug. 2013.

[40] E. E. de Lange *et al.*, "The variaibility of regional airflow obstruction within the lungs of patients with asthma: Assessment with hyperpolarized helium-3 magnetic resonance imaging," *J. Allergy Clin. Immunol.*, vol. 119, no. 5, pp. 1072–1078, May 2007.

[41] B. Driehuys *et al.*, "Imaging alveolar-capillary gas transfer using hyperpolarized 129xe MRI," *Proc. Nat. Acad Sci.*, vol. 103, no. 48, pp. 18278–18283, Oct. 2006.

[42] A. Soliman *et al.*, "Accurate lungs segmentation on CT chest images by adaptive appearnce-guided shape modeling," *IEEE Trans. Med. Imag.*, vol. 36, no. 1, pp. 263–276, Jan. 2017.

[43] M. S. Aslan *et al.*, "Probabilistic shape-based segmentation using level sets," *IET Comp. Vis.*, vol. 8, no. 3, pp. 182–194, Jun. 2014.

[44] T. Koike *et al.*, "Kinetics of lactate metabolism during acellular normothermic ex vivo lung perfusion," *J. Heart Lung Transplant.*, vol. 30, no. 12, pp. 1312–1319, Sep. 2012.

[45] J. M. Charest *et al.*, "Design and validation of a clinical-scale bioreactor for long-term isolated lung culture," *Biomaterials*, vol. 52, pp. 79–87, Jun. 2015.